

Passive WiFi Radar for Human Sensing Using a Stand-Alone Access Point

Wenda Li¹, Member, IEEE, Robert J. Piechocki, Member, IEEE, Karl Woodbridge¹, Senior Member, IEEE,
Chong Tang, and Kevin Chetty¹, Member, IEEE

Abstract—Human sensing using WiFi signal transmissions is attracting significant attention for future applications in e-healthcare, security, and the Internet of Things (IoT). The majority of WiFi sensing systems are based around processing of channel state information (CSI) data which originates from commodity WiFi access points (APs) that have been primed to transmit high data-rate signals with high repetition frequencies. However, in reality, WiFi APs do not transmit in such a continuous uninterrupted fashion, especially when there are no users on the communication network. To this end, we have developed a passive WiFi radar system for human sensing which exploits WiFi signals irrespective of whether the WiFi AP is transmitting continuous high data-rate Orthogonal Frequency-Division Multiplexing (OFDM) signals, or periodic WiFi beacon signals while in an idle status (no users on the WiFi network). In a data transmission phase, we employ the standard cross ambiguity function (CAF) processing to extract Doppler information relating to the target, while a modified version is used for lower data-rate signals. In addition, we investigate the utility of an external device that has been developed to stimulate idle WiFi APs to transmit usable signals without requiring any type of user authentication on the WiFi network. In this article, we present experimental data which verifies our proposed methods for using any type of signal transmission from a standalone WiFi device, and demonstrate the capability for human activity sensing.

Index Terms—Doppler radar, stand-alone WiFi device, WiFi sensing.

I. INTRODUCTION

OVER the last decade, the increase in the aging population has led to a focus on addressing the risks which the elderly are exposed to; from falling down and sudden heart attacks, to longer term conditions relating to mental health, diabetes, and cardiovascular disease [1]. The financial and human resource impacts from these emergency events and

Manuscript received January 29, 2020; revised March 6, 2020; accepted June 24, 2020. Date of publication July 14, 2020; date of current version February 25, 2021. This work was supported by the U.K. Engineering and Physical Sciences Research Council (EPSRC) through the OPERA Project under Grant EP/R018677/1. (*Corresponding author: Wenda Li*)

Wenda Li, Chong Tang, and Kevin Chetty are with the Department of Security and Crime Science, University College London, London WC1E 6BT, U.K. (e-mail: wenda.li@ucl.ac.uk; chong.tang.18@ucl.ac.uk; k.chetty@ucl.ac.uk).

Robert J. Piechocki is with the Department of Electrical and Electronic Engineering, University of Bristol, Bristol BS8 1TH, U.K. (e-mail: r.j.piechocki@bristol.ac.uk).

Karl Woodbridge is with the Department of Electronic and Electrical Engineering, University College London, London WC1E 6BT, U.K. (e-mail: k.woodbridge@ucl.ac.uk).

Color versions of one or more of the figures in this article are available online at <https://ieeexplore.ieee.org>.

Digital Object Identifier 10.1109/TGRS.2020.3006387

medical conditions on healthcare services are significant and need to be addressed using a range of approaches. Daily activity monitoring and behavior recognition in residential and working environments are therefore important for both long-term and short-time tasks, and are extremely useful for preventing chronic diseases and health risks, in which early diagnoses are critical. Compared with the traditional monitoring systems like wearables [2] and camera systems [3], WiFi-based sensing technology is considered as an emerging potential solution for various healthcare applications. The reason is, in part, due to the unobtrusive characteristics of RF-based sensing and ubiquitous nature of WiFi in both residential and commercial environments which can lead to large coverage areas and flexible deployments. Additionally, unlike camera system, wireless signals are not able to generate images of people, which alleviates many privacy concerns.

The fundamental concept around WiFi sensing is that when a person moves, the motion of their body will affect the communication channel in terms of signal attenuation, frequency shift, and propagation paths. As a result, the time-varying communication channel is related to the physical activities which can be used for various purposes like activity recognition and breathing detection. Early approaches use received signal strength (RSS) from WiFi signal [4], however such systems require intensive offline training to assess the surrounding environment and also suffer from coarse resolution. More recently, WiFi-based human sensing systems have been used to measure the WiFi signal variations in the channel state information (CSI) data, yet these systems [5], [6] treat CSI information as a black box. They use machine learning methods to discover the CSI patterns related to certain activities or position, whereas the lack of quantitative models that connect the CSI information to human activities limits the understanding on WiFi signal dynamic and further development of WiFi sensing technology. Furthermore, it is hard to separate useful signal dynamics from the random noise, and most CSI activity recognition systems are constrained to trial-and-error methods when optimizing the system performance [7]. Conversely, passive radar directly outputs a Doppler spectrogram which can be visually analyzed to interpret some basic human motions and can be easily understood for continuous development. Moreover, previous CSI [5], [8], [9] and passive radar systems [10], [11] have used bespoke WiFi devices or high gain antennas with a tapped off reference channel, whereas we use a stand-alone WiFi

access point (AP) as the illuminator without any modified hardware, swapped antennas, or bespoke software.

The term “stand-alone” refers to a WiFi AP without any specific modification, such as an integrated network interference card (NIC), swapped-in high gain antenna for broadcasting, or overwriting the AP’s firmware to setup a high transmission data rate. According to the work in [12], the default beacon interval in commodity WiFi APs is 100 Time Units (1TU = 1024 ns). Some recent work such as [13] and [14] have focused on using passive radar to exploit the WiFi beacon signal but these studies have all increased the repetition rate of the WiFi beacon bursts from the 100 ms default setting to 20 ms (the maximum allowable periodicity on many WiFi APs). These adjustments to make the system usable would again require a level of cooperation with the WiFi AP (in this case password authentication) and therefore cannot be relied on for many real-world deployments. Our previous work shows the feasibility of using continuous WiFi signal for breathing detection [15] and activity recognition [16] with passive radar configuration and Line-of-Sight (LoS) environment. This article further increases the potential of passive WiFi radar to be able work with sparse beacon frame under AP’s idle status and through-the-wall (TTW) scenario.

To cope with the low duty cycles associated with beacon frame transmissions, a modified cross ambiguity function (CAF) is implemented to reduce redundant samples and maximize the use of beacon frame. However, this method only allows a limited Doppler detection due to low amount of effective data. To further improve the detection, an external device has been used to simulate a client device for higher data transmission by talking to the WiFi AP continuously. This device uses the probe request-response protocol in WiFi standard which exchanges information between the WiFi AP and client devices. The probe protocol can be used for requesting the WiFi AP information to increase the bandwidth. Our processing also includes a CLEAN algorithm [17] to remove the strong Doppler peak due to strong direct signal and a constant false alarm rate (CFAR) for target detection.

Compared to previous work [5], [8]–[11], the following contributions are made by this study.

- 1) *Stand-Alone WiFi AP*: Prior to our knowledge, this is the first work study on standalone WiFi AP which has no specific modification to either the hardware and software. With the standalone system, we further extend the usability of WiFi-based sensing for a wider range of use cases.
- 2) *Deal With Beacon Frame*: We overcome the limitation of low-effective WiFi signal during idle status. Two solutions are provided: modified CAF for sparse beacon frame and a client “handshaker” to increase the bandwidth for enhancing performance.
- 3) *Radio Architecture and Proof-of-Concept (PoC) System*: The proposed concepts are built into a software-defined-radio (SDR)-based PoC system. The performance of PoC system is supported by the experiment under TTW scenario with promising results for WiFi sensing.

The rest of this article is organized as follows. Section II outlines related work in WiFi sensing; Section III describes

the basic mechanism of WiFi signal in real-world deployments; Section IV presents the signal processing employed in the standalone WiFi radar system; which is then described in Section V; Finally, experimental results are presented in Section VI and conclusions are given in Section VII.

II. RELATED WORK

Generally, there are two major types of WiFi-based activity capture system, which known as the CSI system (collects channel information) and passive radar system (collects Doppler information).

A. CSI System

A time series of CSI measurements captures the changes of wireless signal travel through surrounding objects and humans in terms of time, frequency, and spatial domain which can be further used for various purposes. Also, different sensing applications have specific requirements of their signal-processing techniques and classification/estimation algorithms. All discussed works in this section are based on the Intel 5300 WiFi NIC.

CSI has been widely used in device-free activity recognition. Work [7] implements an activity monitoring system with a package frame rate of 1500 pk/s. The system contains three receiving channels to monitor at different angle to reduce the limitation of single channel. They also propose a CSI-activity model based on the frequency components of CSI to quantify the relationship between CSI variation and human movement speed to eliminate the effect of environment.

Another work [8] sets the frames rate of 2500 pk/s and collects 2500 CSI values for each of the 180 [2 transmitter antenna \times 3 receiver antenna \times 30 Orthogonal Frequency-Division Multiplexing (OFDM) subcarriers] CSI streams in 1 s. This work uses short-time Fourier transform (STFT) technique to transfer the CSI measurements into spectrogram with covered range up to 14 m. However, data can only be collected on a predefined path in a predefined walking direction, which means a training is required for every new environment of activity.

Fall detection is another interesting area in WiFi sensing. Work [18] demonstrates a system that is able to detect falls automatically from other different activities with a package frame rate of 100 pk/s. It exploits the phase and amplitude changes in CSI, and calculates the power profile in time-frequency domain. But the detection performance is affected by the surrounding environment and location due to the direct signal path.

CSI has also been used for fine-grained finger gesture recognition. Work [19] detects the finger gesture with a much lower package frame rate of 20 pk/s that is more realistic as a real application. It calculates principal components of CSI as the feature vector and classifies finger gesture with dynamic time warping (DTW). This system has a fixed coverage area where the transmitter and receiver are configured as bistatic setup and the target personnel was sitting between them.

Breathing detection by CSI has been shown in [9] with a package frame rate of 20 pk/s. This work quantifies the user

location and body orientation based on Fresnel model with an ellipse shape. It has a similar bistatic setup as [19], whereas the monitoring area is among the middle area between transmitter and receiver.

These works use bespoke WiFi device to collect CSI information, and manually setup a high package frame rate to ensure the bandwidth, which conflicts with the original communication purpose for a WiFi AP. Also, CSI systems are constrained by the changing of surrounding environment which require various degree of training process as well as the transmitter-receiver location toward monitoring target.

B. Passive WiFi Radar System

In addition to CSI systems, passive radar systems have also been used for WiFi sensing. The fundamental aim of passive radar is to use the wireless signal from third-party opportunistic transmitters, and it measures the time difference between the signal arriving directly at the transmitter and the signal arriving via reflection from the object of interest. Different from CSI systems, a typical passive radar contains two coherent channels: a surveillance channel which points to the surveillance area and a reference channel which points to the WiFi AP to reconstruct transmitted signal. Passive radar uses the CAF to calculate range (bistatic distance) and Doppler (bistatic velocity) information. However, due to the bandwidth of WiFi signal is limited (20–40 MHz), normally only the Doppler information has been used for indoor scenario.

An early attempts of passive WiFi radar is shown in [17] which demonstrates the feasibility of using WiFi signal to detect personnel at a stand-off (12 m) distance and TTW scenario. It successfully detects the Doppler of a moving personnel and improves the signal-to-interference ratio (SIR) with a CLEAN algorithm. Its reference channel was been connected directly to the WiFi AP for a perfect signal reconstruction which eliminates the risk of interference.

Work [10] further verifies the passive WiFi radar in an outdoor scenario, and able to correct both range and Doppler information for a moving car and a running human. This work connects a high gain (30 dB), narrow beam (15°) antenna to the WiFi AP to improve the SIR, and puts both transmitter and receiver antenna at same location. This configuration is more like a frequency-modulated continuous-wave (FMCW) radar but transmits WiFi signal.

Lately, work [20] built a prototype base on the SDR platform with low-complexity pipeline design to enable real-time processing ability. This system shows some preliminary results for several applications like TTW activity recognition and finger gesture recognition within laptop area. It has a classical passive radar configuration but assumes that reference channel is stable without any interference from surrounding, and also modified a continuous WiFi signal.

Passive WiFi radar has also been used for vital sign detection, in [15] we demonstrate that the micro-Doppler can be obtained from chest motion as a representative of breathing signal. With appropriate signal processing, it can be further applied to multiple tasks [21]. However, due to the complicated

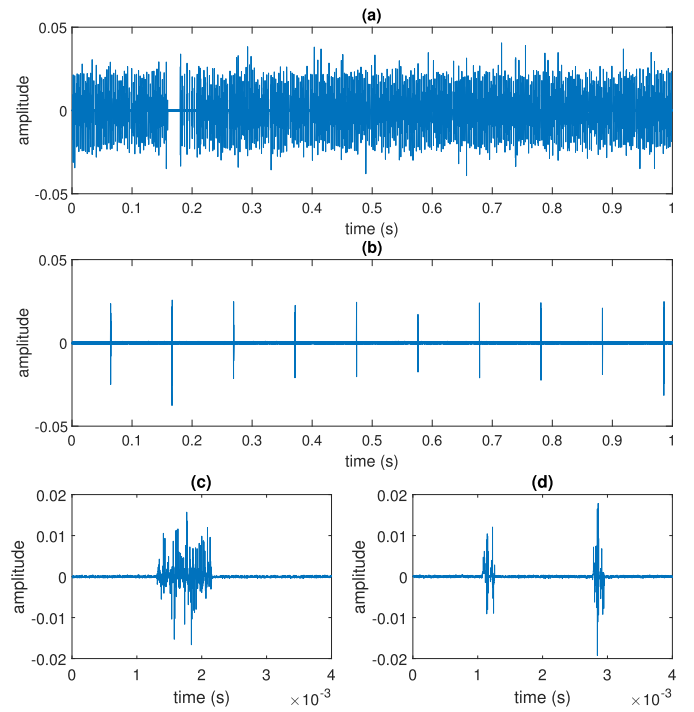


Fig. 1. An example of WiFi status (a) transmission status (full bandwidth WiFi signal), (b) idle status (only contains beacon frame), (c) zoomed-in view of beacon frame, and (d) zoomed-in view of probe request and response frame.

geometry, both [15] and [21] systems are affected by the location among transmitter, receivers, and personnel.

All above works have made some changes to the WiFi AP to enable a high bandwidth signal to broadcast or attached a high gain antenna to the AP. Such configurations are hard to direct applying to real-world scenarios in terms of the bandwidth in communication network and high cost for antenna. In addition, these system geometry are too optimal to be real, like the perfect reference channel and active radar like geometry.

III. WiFi PROTOCOLS FOR SENSING

A. WiFi AP Status

In passive sensing, the WiFi signal is considered as an independent pseudo-noise waveform that is either OFDM modulated for high date-rate communications or a lower-bandwidth signal generated when the WiFi AP is in an idle state. As discussed in Section II, most current WiFi sensing systems [8], [10], [18], [20] rely on the high frame rates to generate sufficient CSI/Doppler information. However, such situation may not always true in case of real life, as communication devices are designed to be bandwidth effective. Here we provide two examples of WiFi signals; first example shows a busy AP which is transmitting data continuously, named as the transmission status; and the second example illustrates the case when there is no internet usage so contains only beacon frames, named as the idle status. The data for both examples were captured for 1 s, and their time domain representations are illustrated in Fig. 1. As shown in the figure, the WiFi signal occupies almost full time domain ($>90\%$) during the transmission status with small time gap.

This provides a large amount of effective data to be used by the passive radar system. In comparison, during idle status, the beacon frame has a small duty cycle with large spaces of redundancy. In fact, manual measurements show that the duty cycle of the beacon frame is 0.42% of that of a data transmission signal. As a consequence, the effective energy one could reuse for processing from the beacon frame is very limited, and as a result the classical CAF processing struggles to work effectively.

B. Beacon and Probe Response Frame

Typically, beacon frames are transmitted periodically to declare the presence of a WLAN with information about the network such as its modulation type, code rate, compatible standards, etc. A wireless enabled device generally scans all RF channels to search for WiFi beacons, which then allows the device to choose to connect the optimal network. Increasing the beacon interval will reduce the load on the network and increase throughput, however it delays the association and roaming processes. Alternatively, decreasing beacon interval decreases throughput for users and increases the network load. A zoomed-in view of beacon frame is shown in Fig. 1(c) with a duration less than 0.5 ms.

The WLAN clients use probe request frames to scan the area for availability of WLAN network. In response to the received probe request, the network sends out a probe response frame when parameters are compatible. Probe response frames are exclusive to physical layer in use as mentioned in beacon frame. A zoomed-in view of probe request and response frame is shown in Fig. 1(d). As it can be seen, the first frame with lower amplitude is a probe request signal and the second is probe response frame due to WiFi AP has higher transmission power. In this work, we use a client simulator to trigger probe request and response frames at relatively high transmission rates. This approach is similar to the mechanism in CSI system but avoids any firmware modifications and hardware changes for WiFi AP.

Both the beacon and probe response frames are not encrypted in IEEE 802.11 family of standards. The difference is that the beacon frame broadcasts constantly from a WiFi AP, whereas probe response signal is a response to the client device. Both signals can be used for opportunistic sensing, but their performance depends on the amount of effective data. The duration of beacon and probe response frame are varied depending on the standard, setting, and information contained.

C. Monitoring a Public Access WiFi AP

To better understand the WiFi usage in a real scenario, we use the WiFi network analysis tool “Wireshark” to monitor the WiFi traffic from the “Eduroam” wireless network over a 24-h period. Eduroam is an university wide WiFi network and the AP of interest was located in an office consisting of an approximately 40 staff and students who are present during typical office hours. The transmitted frame number versus frequency of occurrence is shown in Fig. 2. It is found that even during the working hours (between 9 A.M. and 5 P.M.), the peak is around 100 frames/s which is much lower than the

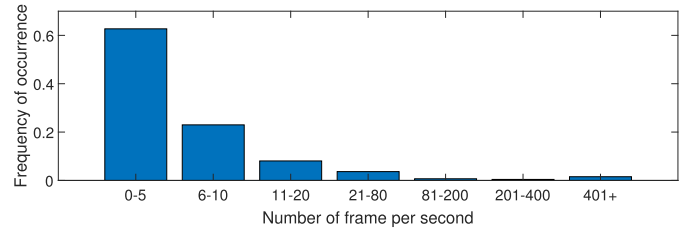


Fig. 2. Frame rate captured over 24-h period.

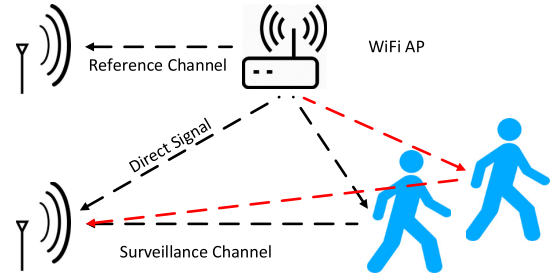


Fig. 3. Passive WiFi radar sensing.

request frame rate in the previous activity recognition work [7], [8], [19]. Outside of working hours, the frame rate drops to around 4–5 frames/s which is of similar order to the beacon frame rate. In addition, it is reasonable to assume WiFi usage in a residential area will be lower than this level due to lower user numbers. Thus, it is necessary to consider the effect of low frame rates when designing a real WiFi sensing system.

IV. SIGNAL PROCESSING FOR PASSIVE WiFi RADAR

A. Preliminary of Passive WiFi Radar

Passive radar systems employ two synchronized receiver channels; the surveillance channel records reflected WiFi signals from the monitoring area while the reference channel records the signal from the transmitter. In a typical indoor scenario, as illustrated in Fig. 3, WiFi transmissions propagate through the space and the signal environment is characterized by both the topology and the clutter. If a person is present in the environment, additional changes are introduced to the signal which correspond to the effects of human presence in the environment. If there is no one or no motion in the environment, the signal will be relatively stable. However, as shown by the red lines in Fig. 3, along with the person moving to a new location, the geometry of passive radar system is changing which results in the change of amplitude attenuation and phase shift in WiFi signal.

B. Collecting Doppler Information

In IEEE 802.11 standard, signals are modulated by OFDM scheme [22]. This also applies to the beacon and probe response signal. Let the transmitted OFDM signal defined as

$$x(t) = \frac{1}{\sqrt{N}} \sum_{n=0}^{N-1} a_n e^{j2\pi n t} \quad (1)$$

where N is the number of OFDM symbols for each carrier a_n and n is the index of OFDM symbol. The received signal

$y(t)$ consists of both direct signal and target reflections. These reflections from a stationary clutter or a moving person can be described by a summation of delayed and phase shifted transmitted signal. The received signal can be written as

$$y(t) = \sum_p A_p e^{j2\pi f_d f_c t} x(t - \tau) + n(t) \quad (2)$$

where p is the number of reflected paths, and A_p , τ , f_d are the attenuation factor, delay, Doppler shift for p th path, respectively, $n(t)$ is the additive white Gaussian noise (AWGN).

In passive radar, CAF processing is commonly used to obtain the range τ and Doppler f_d information by taking fast Fourier transform (FFT) of cross-correlated signals from surveillance channel $S_{\text{sur}}(t)$ and reference channel $S_{\text{ref}}(t)$. In terms of a passive WiFi radar, $S_{\text{sur}}(t)$ represents the $y(t)$ which is collected from the surveillance area and $S_{\text{ref}}(t)$ recreates the transmitted signal $x(t)$ without any interference as possible. In this case, CAF equation can be written as

$$\text{CAF}(\tau, f_d) = \int_0^{T_i} S_{\text{sur}}(t) S_{\text{ref}}^*(t - \tau) e^{j2\pi f_d f_c t} dt \quad (3)$$

where T_i is the integration time which defines the Doppler resolution as: $\Delta f_d = 1/T_i$, $*$ is the complex conjugate. However, above equation requires a high computational load which prohibits our system for operating in real time. Thus, a batch-processing technique [20] has been used for complexity reduction. This is achieved by dividing a long sequence into several short batches so that the cross correlation and FFT process over each batch are faster.

One of the limitations of (3) is that it cannot generate meaningful Doppler signature during the idle status [see Fig. 1(b)] due to the ultralow-density of the beacon signal, as well as the high amount of redundant noise. To that end, the modified CAF is proposed to maximize the effective data contained within the beacon signal. The idea is to synchronize and extract the beacon signal before them passing to the CAF. This can ensure only useful data are collected and processed, whereas the noisy data can be filtered out. In this work, beacon synchronization is implemented based on the energy curve X_i which is calculated as the cumulative sum of the absolute value of WiFi signal. Then the normalized energy curve X'_i as suggested in [23], is calculated as

$$X'_i = X_i - i\delta = \sum_{k=0}^i (x_k^2 - i\delta) \quad (4)$$

where k is the index of signal, i is loop variable ranging through all samples. δ is a negative trend and depends on the total energy of the selected signal X_{N_e} with window length of N_e as determined by $\delta = (X_{N_e}/\alpha \cdot N_e)$. In this work, N_e is the length of signal of one integration time T_i .

A demonstration of 1-s beacon synchronization is shown in Fig. 4. The energy curve for beacon signal Fig. 4(a) is calculated in Fig. 4(b), and the corresponding normalized curve is plot in Fig. 4(c). Afterward, we search the smallest value within each beacon interval as the start time of a beacon frame, for example, Fig. 4(c) is an example of 100 TU. Afterward, the modified CAF with synchronized beacon signal

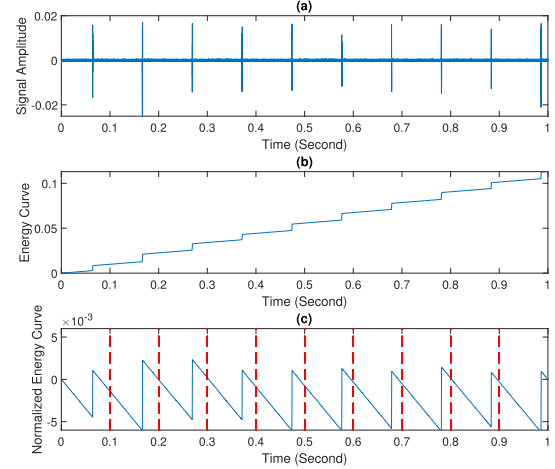


Fig. 4. Beacon synchronization process. (a) Example of WiFi beacon signal. (b) Energy curve for beacon signal. (c) Corresponding normalized curve.

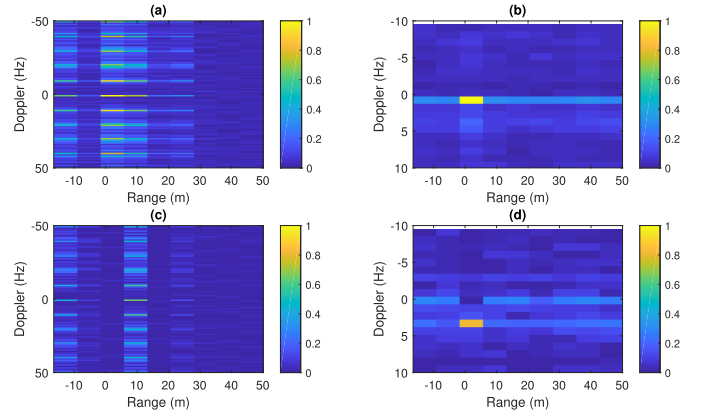


Fig. 5. Example of CAF surface during WiFi idle status (a) classical CAF (3), (b) modified CAF (5), (c) classical CAF with CLEAN algorithm, and (d) modified CAF with CLEAN algorithm.

can be written as

$$\text{CAF}(\tau, f_d) = \sum_{n=0}^{N_b-1} \int_0^{T_b} S_{\text{sur}}^n(t) S_{\text{ref}}^{n*}(t - \tau) e^{j2\pi f_d f_c t} dt \quad (5)$$

where, N_b is the batch number and is equivalent to the number of Doppler bins or the number of beacon, T_b is the time duration of each batch or the duration of a beacon, and n is the index of batch. To optimize performance, the beacon synchronization is designed based on the signal recorded in the reference channel as it has a higher SNR and is subject to less fluctuations than the signal measured in the surveillance channel. It is noted that there are still interference components in reference channel (for example, other data packets or from a WiFi AP transmitting in the same frequency band), which may lead to synchronization distortions.

Examples of a CAF output surface using classical CAF (3) and modified CAF (5) after processing the beacon signal are shown in Fig. 5(a) and (b). These data are captured from a walking person. As it can be seen, there are significant sidelobes in both Doppler and range on CAF surface with classical CAF, and no meaningful information can be extracted.

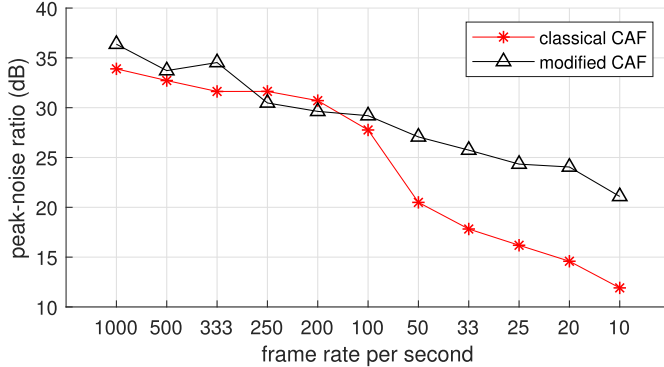


Fig. 6. PNR versus frame rate.

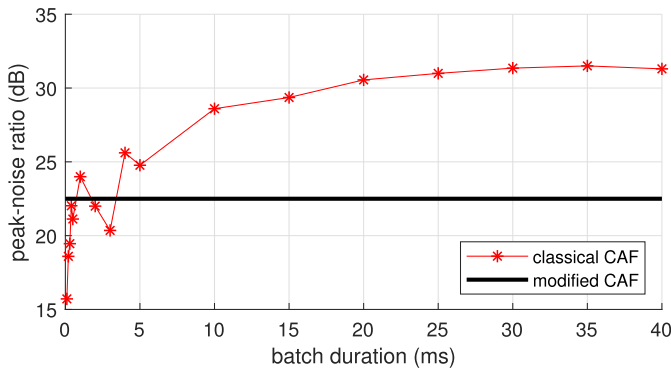


Fig. 7. PNR versus the batch duration.

We attribute this output to the sparse nature of beacon frame. For this reason, the modified CAF is applied. Visual inspection of the output shows a much cleaner surface with a dominant peak at zero range/Doppler bin. It is noted that the boundary of Doppler is limited in sparse mode since there are only ten WiFi beacon bursts available in each second which can be used in the batched processing. This means the maximum detectable boundary is five Doppler bins for 1 s (in both positive and negative domain). To better demonstrate the Doppler pulse, the integration time T_i for sparse mode was set as 2 s so that twenty beacons are available in the range-Doppler surface.

To further demonstrate the effect of frame rate in the CAF processing, the peak-noise ratio (PNR) between the dominant Doppler peak and rest CAF surface is measured. Higher PNR generates a higher quality Doppler spectrogram. For modified CAF, the frame rate also determines its batch number N_b , where the classical CAF has a constant $N_b = 100$. The PNR plot of both CAF processing are shown in Fig. 6. As it can be seen, there is a significant improvement of proposed modified CAF, in average, modified CAF delivers 8-dB higher PNR than the classical CAF between 10 and 50 frame rate. PNR values become similar after 100 frame rate with very small difference between two CAF processing.

Another important factor is the batch duration T_b which defines the length of data used for the cross correlation processing, and also affects the noise level in CAF surface. Generally, a longer batch duration leads to a lower noise level, but requires more computational power. A plot of PNR versus batch duration is shown in Fig. 7. As it can be seen, PNR of

the classical CAF improves gradually until 10 ms then remains constant thereafter. For the modified CAF, PNR is constant because the duration of beacon signal is fixed at 0.8 ms. In this work, batch duration of both enhanced mode and transmission status were set as 10 ms to fully use the received data, that is $T_i(1s) = N_b(100) \times T_b(10ms)$.

C. Cancellation of the Direct Signal Interference (DSI)

The surveillance channel of a passive radar system consists of a DSI component, target clutter, Doppler-shifted target echoes, and thermal noise. The expression of received signal in surveillance channel can be written as

$$S_{\text{sur}}(t) = S_{\text{dsi}}(t) + S_{\text{clutter}}(t) + S_{\text{tar}}(t) + n(t) \quad (6)$$

where $S_{\text{dsi}}(t)$ is the signal from direct path, $S_{\text{clutter}}(t)$ is the signal reflected from surrounding clutter, and $S_{\text{tar}}(t)$ is the signal reflected from target. Replacing $S_{\text{sur}}(t)$ in (6) with its full expression from (5) allows the final CAF surface to be written as the sum of the CAF surfaces of each components as

$$\begin{aligned} \text{CAF}(\tau, f_d) = & \sum_{l_1=1}^{L_L} \text{CAF}_{\text{dsi}}^{(l_1)}(\tau, f_d) + \sum_{l_m=1}^{L_M} \text{CAF}_{\text{clutter}}^{(l_m)}(\tau, f_d) \\ & + \sum_{l_n=1}^{L_N} \text{CAF}_{\text{tar}}^{(l_n)}(\tau, f_d) \end{aligned} \quad (7)$$

where CAF_{dsi} , CAF_{tar} , and CAF_n are the CAF surface due to DSI, target, and noise, respectively. L_L represents the number of reflected paths due to DSI, L_M represents the number of reflected paths due to the surrounding clutter and L_N represents the number of reflected paths due to the target. We note that in (7), item $\sum_{l_1=1}^{L_L} \text{CAF}_{\text{dsi}}^{(l_1)}(\tau, f_d)$ would be expected to generate a main peak in the zero Doppler bins, whereas item $\sum_{l_m=1}^{L_M} \text{CAF}_{\text{clutter}}^{(l_m)}(\tau, f_d)$ can produce both range and Doppler sidelobe responses.

There are two types of technique to implement the CLEAN algorithm for removing the effect from DSI and stationary clutter, known as preprocessing and postprocessing. Preprocessing techniques aim to perform subtractions in the signal domain rather than in the CAF surface; however, this process requires significant computational power considering the size of raw WiFi signal received by SDR system. Alternatively, postprocessing method subtracts the interference at CAF surface, and is a less complex approach requiring lower computational power. We therefore focus more on postprocessing techniques to achieve real-time outputs.

In this work, we adopt the method suggest by [17] with a shifted magnitude-scaled and phase-corrected version of the self CAF surface to provide a model of the cross-ambiguity surface. Let $\text{CAF}^k(\hat{\tau}, \hat{f}_d)$ represents the cleaned CAF mapping at k_{th} iteration, it can be written as

$$\text{CAF}^k(\hat{\tau}, \hat{f}_d) = \text{CAF}^{k-1}(\tau, f_d) - \alpha^k \text{CAF}_{\text{self}}(\tau - T_k, f_d) \quad (8)$$

where α^k is the maximum absolute value of $\text{CAF}^k(\tau, f_d)$, T_k is the phase shift factor refers to the α^k . CAF_{self} is the self CAF over the reference channel. The phase of $\text{CAF}^k(\hat{\tau}, \hat{f}_d)$ is shifted by multiplication with a complex phasor $e^{j\Delta\phi}$,

where $\Delta\phi$ is the difference in phase between the peak in $\text{CAF}^k(\hat{\tau}, \hat{f}_d)$ and the peak found along the zero Doppler bin. From observation, one iteration ($k = 1$) is sufficient for our system.

The cleaned CAF surface of Fig. 5(a) and (b) are shown in Fig. 5(c) and (d), respectively. For classical CAF, even after the CLEAN algorithm, there is still no meaningful Doppler information. In contrast, the dominant peak in modified CAF surface has been successfully removed. As a result, the desired peak is present clearly on the map at 5 Hz which corresponds to the person's velocity.

Afterward, a Doppler spectrogram $D(f_d, t)$ is generated by extracting one column with maximum value in the CAF surface.

D. Motion Indicator

In this work, we consider a person as being in one of two states: an active state (e.g., walking, body swing, and other types of full/part body movement) and a stationary state such as sitting or standing still, where only the motion of the chest wall during breathing is detectable. Thus, it is necessary to distinguish these two periods, since their Doppler signatures are significantly different.

This is based on the fact that human movements generate much higher power in terms of Doppler pulse. When there are no human movements, the power in Doppler spectrogram is mostly low since there is no frequency shift in the surveillance channel. In this work, we consider it as a pulse detection problem by estimating the noise level $\hat{N}(t)$ using a moving average (MA) algorithm during the stationary period as $\hat{N}(t) = (1/w) \sum_{t=0}^w |D(f_d, t)|^2$, where w is the window length which is set as 5 s.

We set the detection threshold as four times of the noise level, so that a movement can be detected when the Doppler power deviates from the average noise level. Once a movement is detected, we use a standard CFAR algorithm to detect the Doppler response associated with a moving person, and record the spectrogram.

E. Breathing Response

During stationary periods, the velocity of the chest wall is considerably lower than that of body movements. Detection of the periodic chest wall motion associated with breathing can therefore be achieved with a higher Doppler resolution by extending the integration time T_i used in (3). However, the target's velocity is assumed constant during the period of integration time whereas this is not suitable for our system to capture fast movement. Thus, we use a micro Doppler extraction method to extract the breathing signal $B(t)$ while maintaining the Doppler resolution as normal. The idea is to use the macro imbalance between the Doppler positive and negative domain caused the chest motion

$$B(t) = \sum_{f_d=-\frac{1}{2}\text{MAX}\{f_d\}}^{\frac{1}{2}\text{MAX}\{f_d\}} D(f_d, t)(n) * \left\lceil \frac{\text{MAX}\{f_d\}}{2} - i \right\rceil \quad (9)$$

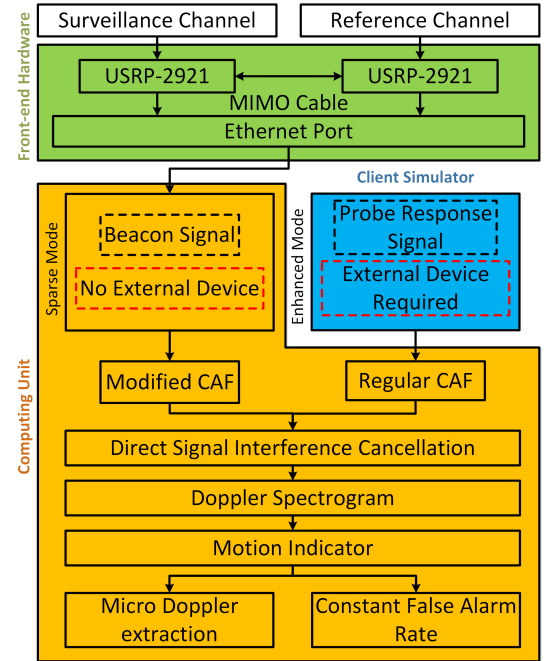


Fig. 8. Block diagram of proposed system.

where i is the index of Doppler bin, $\text{MAX}\{f_d\}$ represents the maximum of Doppler bins in Doppler spectrogram $D(f_d, t)$, it is equivalent to the number of beacon in terms of sparse mode and was set as 100 in terms of enhanced mode and during transmission status. When the target is in stationary, the breathing response signal $B(t)$ can be obtained directly from the spectrogram as it only contains chest movement.

F. Target Detection

A CFAR threshold has been used to detect the target in CAF surface and further reduce the levels of noise and interference. There are multiple interference sources which may arise from: incorrect beacon synchronization that captures an ineffective signal; interference from WiFi signals from other AP; and other packet transmission interrupting the beacon synchronization

$$\Lambda = \frac{1}{N_r \cdot N_{f_d}} \sum_{i=1}^{R_r} \sum_{j=1}^{R_{f_d}} \text{CAF}(\tau_i, f_d j) \quad (10)$$

where Λ is the threshold mapping for CAF. i and j are the index for range and Doppler bin, N_r and N_{f_d} are the training length in range and Doppler bin, respectively. This threshold mapping is then used for normalizing the power and remove the noise as $P(i, j) = |\text{CAF}(i, j)|^2 / \Lambda$. For $P(i, j) < 1$ are considered as noise and replaced with zeros, others are considered as activities.

The effectiveness of above signal processing will be presented in Section VI.

V. SYSTEM IMPLEMENTATION

A. System Overview

The proposed passive WiFi radar system is implemented based on the popular Universal Software Radio

TABLE I
SYSTEM PARAMETERS FOR EACH MODE

	sparse mode	enhanced mode	transmission status
WiFi signal	beacon frame only (100 TU, default setting)	probe response frame (13 TU)	data frame (varied time gap, base on the internet usage)
effective data integration time T_i	around 0.4%	around 18%	around 90%
number of batch N_b	20	100	100
batch duration T_b	0.8 ms	10 ms	10 ms
maximum detectable velocity $\max\{f_d\}$	0.625 m/s (cannot increase)	6.25 m/s (can increase)	6.25 m/s (can increase)
bandwidth	1M	1M	1M

Peripheral (USRP) platform. The overall block diagram of our passive WiFi radar is presented in Fig. 8. It contains mainly three parts: radio frequency front-end, passive radar signal processing, and a client simulator.

The front-end hardware uses two NI USRP-2921 [24] each contains a tunable RF transceiver for acquiring the wireless signal and two ADCs for digitization. An MIMO-cable is used to share the clock source between two USRPs to synchronize the reference and surveillance channel. Surveillance channel is equipped with a 18-dB Yagi antenna, and reference channel is equipped with a 14-dB Yagi antenna. The collected raw data are then transmitted to a computing unit, which is a laptop in this work, through an Ethernet port. It is noted that the NI-USRP is a tool which allows rapid prototyping and testing, a real-world passive WiFi sensing system would require lower technical specification and a less complex radio architecture making it significantly lower cost.

The key feature of our system is the capability of using standalone WiFi AP for personnel monitoring. Thus, a modified CAF [using (5)] and a client simulator are implemented to cope with the sparse beacon signal. The signal processing for passive radar described in Section IV is implemented with LabVIEW. It first calculates the CAF surface from either sparse or enhanced mode based on the quality of the Doppler signature and the density of WiFi signal. Afterward, a motion indicator identifies the activity level and chooses the desired output. A pipeline structure [15] has been used to divide the long serial signal processing of passive radar signal processing into short parallel processing. This structure allows the system to run in real time on a laptop.

The client simulator adopts the idea of probe response protocol to generate higher bandwidth with more effective signal. In our system, it is used aligned with the enhanced mode during WiFi idle status. This device can be activated when there is a need of detailed detection during the WiFi idle status. It is noted that the regular CAF is also applied to WiFi transmission status as it has high frame rate.

Table I summarizes the system parameters for our passive WiFi radar system. The maximum detectable velocity can

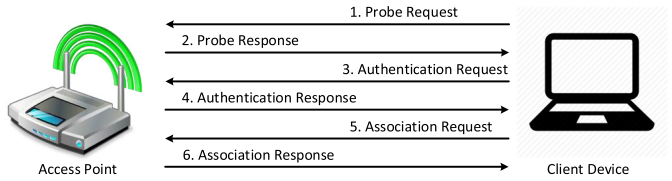


Fig. 9. Life-cycle of probe response signal.

be calculated as: $\max\{f_d\} = N_b \times \Delta f_d \times f'/2$, where $\Delta f_d = (1/T_i)$ is the Doppler resolution and $f' = (c/f_c) = (3 * 10^8 / 2.4 * 10^9)$ is the relative velocity corresponding to each Hz in Doppler which is 0.125 m/Hz. The factor 2 is used for representing both positive and negative domain. The major limitation of sparse mode is the maximum detectable velocity (0.625 m/s) which is due to the number of beacon of frame as 10 frames/s. To better demonstrate the Doppler signature, we use 2 s of integration time T_i in sparse mode to double the N_b but half the Δf_d . Thus, the $\max\{f_d\} = N_b$ remains the same. In comparison, enhanced mode has no limitation on maximum detectable velocity by having higher N_b as in (3).

B. Implementation of Client Simulator

A Raspberry Pi running Kali Linux has been developed to stimulate a client device which continuously sends probe request frames to the target WiFi AP. The waveform of a response frame is shown in Fig. 1(d). It is processed according to the 802.11 protocol [25] and includes three consistent request frames and three response frames as shown in Fig. 9. To avoid the mechanism in WiFi protocol that prevents a device repeatedly sending the request frame, the client simulator changes its media access control (MAC) address after each probe request is sent.

In our tests, the maximum achievable frame rate for current setup is 75 probe requests per second (approximately 13 TU) which provides much higher density than the default setting of beacon signal (100 TU). A higher frame rate could be achieved with more powerful system like a WiFi NIC. Despite the enhanced mode being able to generate a large amount of effective data to be used by our passive WiFi radar system, the bursty nature of probe response signal means there are still considerable time gaps when compared with the WiFi transmission status [see Fig. 1(a)].

VI. EXPERIMENTAL RESULTS

The test area consisted of an individual room of dimensions 4.3 m \times 4.6 m, separated by a 16-cm thick wall made of both brick and plasterboard. A standalone WiFi AP (Model: DWL-2000AP+) was placed in the corner of the test area whilst the passive WiFi radar system was located outside of the room. The reference and surveillance antennas were directed toward the WiFi AP and center of the room. A large file was transmitted through the WiFi AP for experiments which required high-data rate signal transmissions; termed transmission status. For experiments which required only WiFi beacon signal transmissions; termed the idle status, the WiFi AP was left alone. This respective WiFi signal transmissions

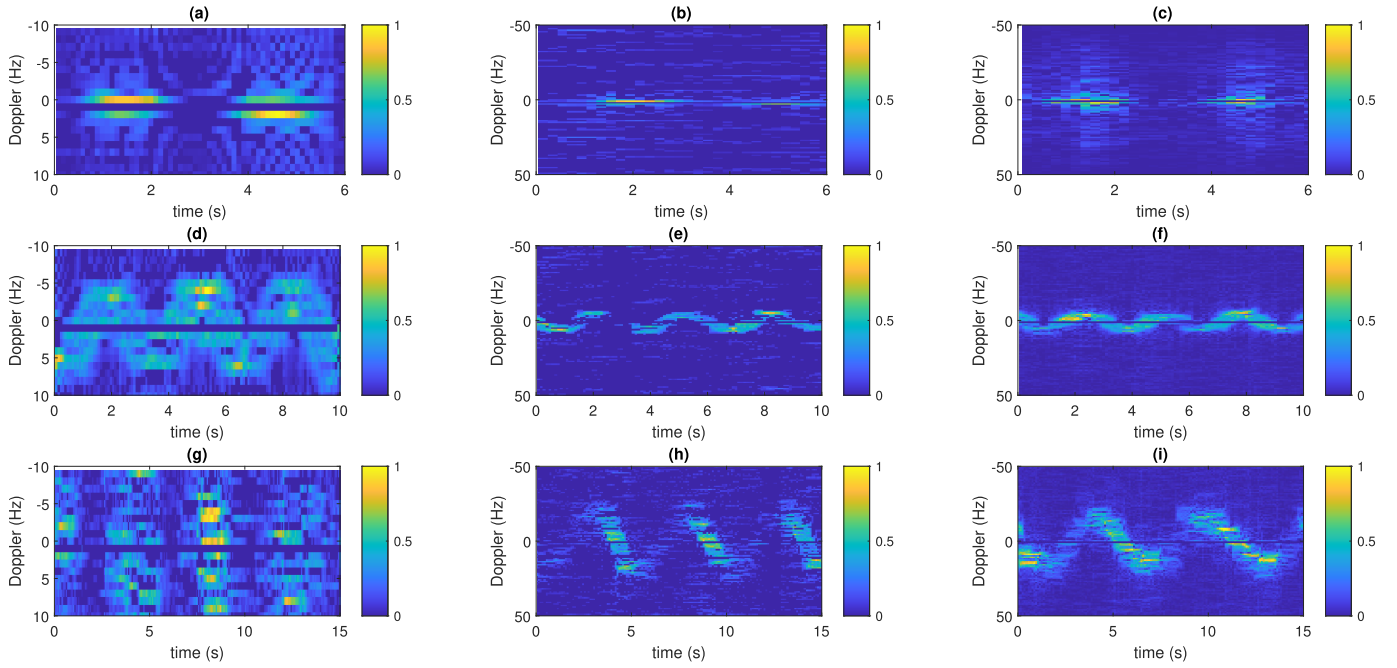


Fig. 10. Doppler spectra examples: sitting still in (a) sparse mode, (b) enhanced mode, and (c) transmission status; body swing in (d) sparse mode, (e) enhanced mode, and (f) transmission status; and walking in (g) sparse mode, (h) enhanced mode, and (i) transmission status.

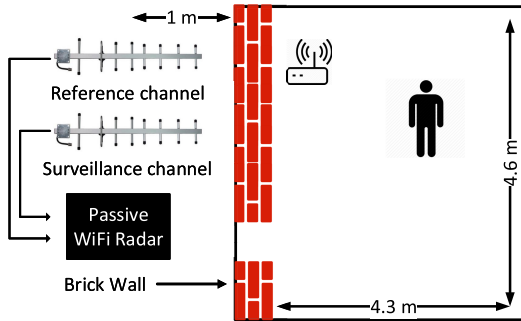


Fig. 11. Experiment layout.

are illustrated in Fig. 1(a) and (b), and the experimental layout is shown in Fig. 11.

A. System Mode Comparison

We first demonstrate our system's detection performance with different WiFi signal density, or duty cycles. We compare the Doppler signature during the WiFi idle status with both sparse and enhanced mode, and during the data transmission status. The transmission status is considered as the optimum signal for sensing (given the current settings) and this "gold standard" is as the baseline reference when comparing to the other two modes in idle status.

Three activity classes are measured to demonstrate the feasibility of our passive WiFi radar system. Each activity consists of different motion velocities. For example, standing still encompasses a slow movement of the chest during breathing, body swing involves rocking on the spot with a medium velocity, and walking forward and backward within surveillance

area typically consists of a wider range of faster motions. All obtained Doppler spectrograms are shown in Fig. 10. As can be seen, sparse mode can give the correct Doppler pattern for breathing and body swing. The two peaks in Fig. 10(a) in both the positive and negative domain represent the Doppler change during the process of inhalation and exhalation. Also the sinusoidal wave in Fig. 10(d) shows the periodic characteristics associated with body swinging. Despite the fact that some noise appears in the spectrogram, the overall Doppler shape is distinguishable. As discussed before, the major limitation of the sparse mode is the maximum detectable velocity. This happens when a faster activity is performed, for example walking. Fig. 10(g) illustrates a Doppler signature that is difficult to interpret because of the walking speed goes beyond the Doppler boundary and appears in the other side of the Doppler domain, from the maximum positive Doppler bin to the negative domain or another way. In such a case, the sparse mode of passive WiFi radar can simply act as a motion detector.

Enhanced mode can be then activated for a better detection with the client simulator. Benefits of the higher frame rate, spectrogram in Fig. 10(b), (e), and (h) shows improved Doppler signature when compared to sparse mode. All three activities are clearly captured with distinguishable traces. However, there are some noise spread at different Doppler bins among the spectrogram. This is because of the time gap between the probe response frame that induces errors among correlation and FFT in CAF process.

As expected, transmission status delivers the best performance in all scenarios. It outputs clear Doppler signature for all three activities and with lowest noise level in spectrogram. There are even some micro-Doppler can be seen across the

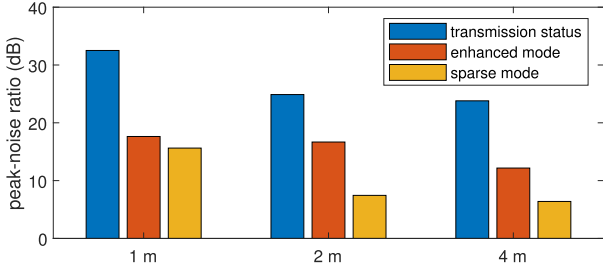


Fig. 12. Sensitivity of breathing detection at different distances.

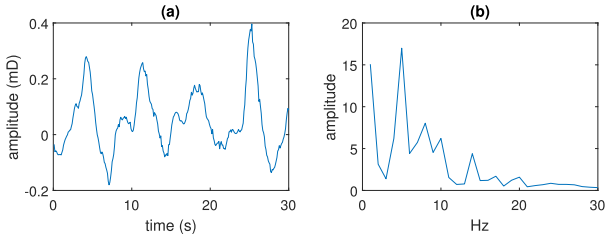


Fig. 13. (a) Breathing signal from micro-Doppler. (b) Breathing rate from FFT.

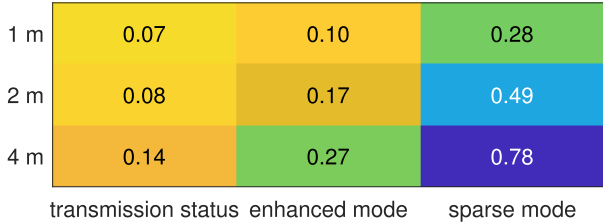


Fig. 14. Error rate of detected breathing rate versus distance.

walking activity in Fig. 10(i). But still, enhanced mode can provide close performance compare to that from transmission status.

B. Breathing Detection

To verify the sensitivity of the proposed system for breathing detection, a subject stood still and faced the surveillance antenna. Limited by the room size, the experiment was carried out at 1, 2, and 4 m away from the wall under all three modes. We calculate the PNR of the Doppler peak which is caused by the chest movement and with the background noise in CAF surface. A higher PNR corresponds to an increased probability of detecting a breathing signal from the Doppler spectrogram, whereas a low PNR means more noise. The results are shown in Fig. 12. As expected, the transmission status shows the best performance, following with the enhanced mode and sparse mode. The extracted breathing signal and rate suggests that breathing detection in transmission status is capable of covering the entire room, whereas enhanced mode and sparse mode can only cover part of the room.

We have shown the Doppler spectrogram for breathing detection in Fig. 10(a)–(c). Here, (9) was applied to the Doppler spectrogram to extract the breathing signal. Fig. 13(a) shows an example of a 30-s breathing signal extracted from Doppler spectrogram. The exhalation and inhalation phases

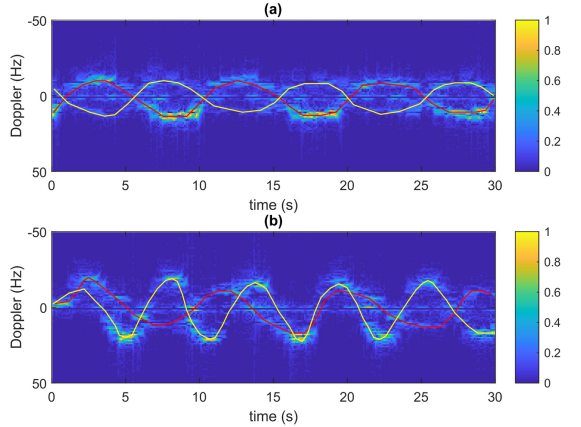


Fig. 15. Example of two people walking (a) same velocity, opposite direction, and (b) different velocity, varying direction. The red and yellow lines are the Doppler trajectory for each person.

of breathing can clearly be identified. Parameters such as the signal amplitude, frequency, and periodicity in the breathing response can be potentially used for the identification of the subject's health condition [26]. A simple FFT was used to calculate the breathing rate, shown in Fig. 13(b), which corresponds to the breathing signal in (a). We pick the maximum absolute value of the output as the frequency of the breathing rate, and avoid the first frequency component which may contain high noise. The dominant peak clearly indicates four repetitions (in 30 s) which equivalents to 8 breaths/min.

2 min of breathing measurement were captured from each status, and the person was asked to breathe at a constant rate by counting the time. The rate of breathing rate was calculated over 30 s with a moving window of 1 s, which is expected to be constant for each measurement. We calculate the error rate for each scenario as shown in Fig. 14. It can be seen that the best error rates are obtained with transmission status for all distances, whereas enhanced mode shows close error rates but slightly worse. Sparse mode has the worst performance and is unable to correctly detect the breathing rate beyond 2 m.

C. People Counting

Person detection experiments are typically based on data generated by a single person. However, the presence of multiple people is a more realistic in a real-world scenario. One such application scenario is the ability to count the number of people in locations like a shopping mall, train station, or airport. Work [27] developed a WiFi CSI system to count a group of walking people; however, this type system needs regularly calibration to cope the changing of surrounding environment. In comparison, our passive WiFi radar system does not require any calibration and provide meaningful Doppler signature. Enhanced mode was used in this experiment, since the sparse mode is not able to detect walking correctly as presented in Fig. 10(g).

Fig. 15(a) shows two people walking in same velocity but opposite direction in a straight line, for example, one walk forward to the surveillance antenna while another one backward. The Doppler trajectory for each person is also

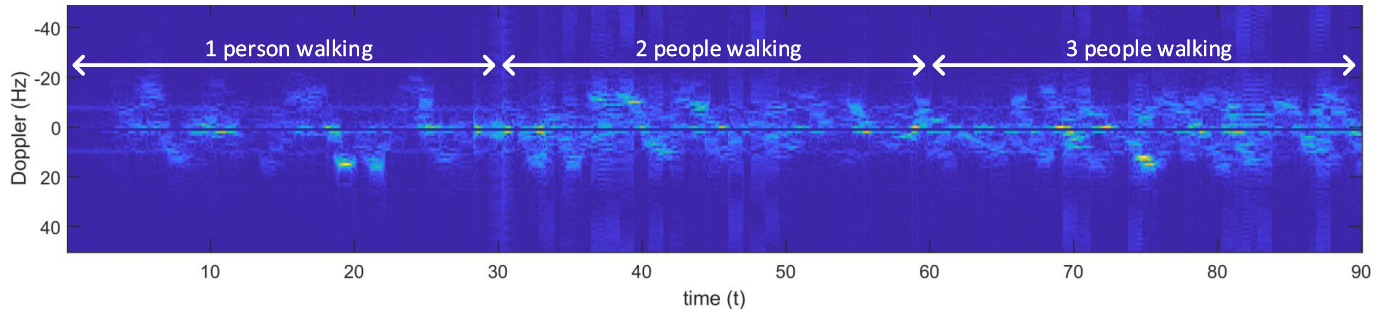


Fig. 16. Example of a random walk for (a) one person, (b) two people, and (c) three people.

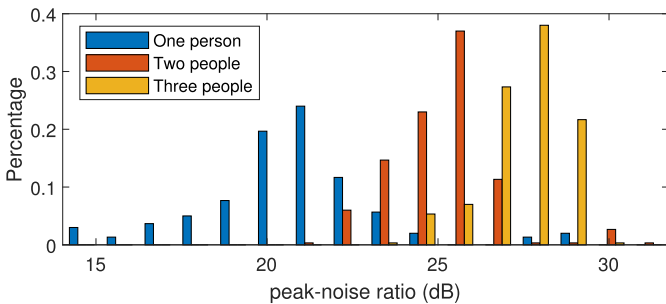


Fig. 17. Histogram of PNR distribution for one, two, and three people.

labeled in different color. As it can be seen, there are two sinusoidal Doppler signature in the spectrogram, each represents a trajectory for one person. The Doppler signature for both person are clear with same periodicity and velocity, and almost identity direction. Fig. 15(b) shows two people walking in different velocity and remaining in a straight line. The spectrogram shows two sinusoidal Doppler signature but with different periodicity and velocity. These results show how the velocity of two people would affect spectrogram. Such Doppler spectrogram could potentially provide velocity for indoor tracking with proper tracking filter.

To simulate a more realistic scenario and demonstrate the difference in the number of people, maximum three people were asked to enter into the experiment room and walk in random direction. The Doppler spectrogram for random walking is shown in Fig. 16. As it can be seen, the Doppler signature is much random and no longer a sinusoidal wave as its direction is not in a straight line. Based on the velocity and duration, it can be easily distinguished from other body activities like a body swing. We can also see obvious difference in Doppler signature among the one person, two people and three people walking. One person shows a simple Doppler signature with a single trajectory, whereas two people have more complicated trajectory and three people show the most messy trajectory. This can be understood use the principle discussed in Fig. 15 that the Doppler spectrogram is a combination of multiple Doppler signature from each moving person. By calculating the number of Doppler signature within certain period, it is possible to count the number of people. Such results could also be used for applications like people counting.

Fig. 17 shows the PNR distribution in Doppler spectrogram as in Fig. 16. These distributions clearly show the difference

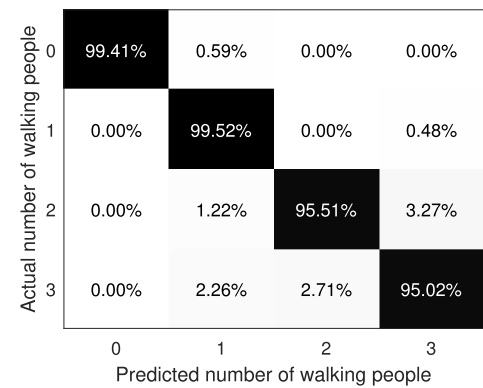


Fig. 18. Confusion matrix of people counting.

for different number of people walking. The one person case has the lowest PNR value, while three people walking has the highest PNR value. This is because of the multiple Doppler peaks which contain a higher PNR value than the single Doppler peak. To further verify the accuracy of people counting, a 10-min measurements of one, two, and three people walking in a room were collected, including a control measurements for when the room was unoccupied. The resulting spectrograms were segmented into small samples consisting of a window size of 0.5 s. In total 5051 samples were acquired, among them 4206 were used as training samples and 845 were used as testing samples. A simple LeNet neural network [28] was used as the classifier. The classification results are shown in Fig. 18, with an overall accuracy of 97.37%. All classes reach more than 95% accuracy, especially the empty room and one person walking classes, which both are more than 99%. The accuracy for multiple people walking slightly decreases to around 95% but remains at high level. Such performance illustrates the application potential for the proposed system to be used in occupancy detection and counting.

D. Weak Reference Channel

One of the major challenges of our passive WiFi radar system is the stability of the reference channel. Consider in a real scenario, the reference channel may not always as strong as the experiment layout shown in Fig. 11. When the antenna is not pointing to the WiFi AP directly, reference channel becomes weak that could bring additional noise to the CAF surface. Thus, it is necessary to examine the detection

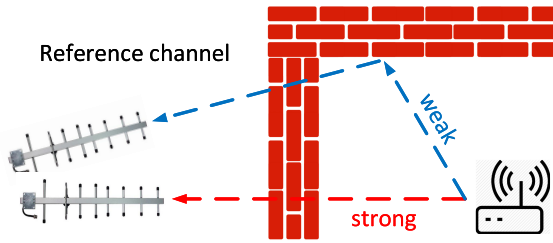


Fig. 19. Example of strong and weak reference channel.

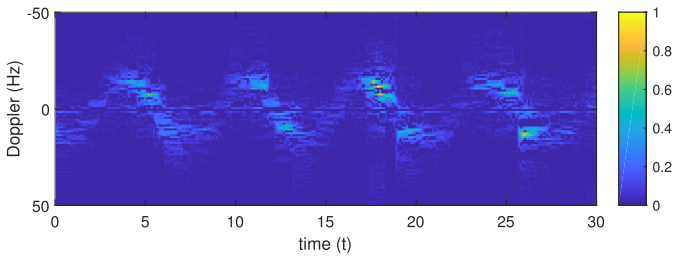


Fig. 20. Doppler spectrogram of walking activity with weak reference channel.

performance under weak reference channel. A typical layout of strong and weak reference channel is illustrated in Fig. 19. Recall the CAF processing in (3), it assumes reference signal S_{ref} perfectly recreate the transmitted signal from WiFi AP without time delays and Doppler shift. In terms of weak channel, additional time delay τ_0 (from wall reflection) is added into the S_{ref} . CAF surface with weak reference channel can be then rewritten as $\text{CAF}(\tau + \tau_0, f_d)$. Since τ_0 does not affect the Doppler measurement, our passive WiFi radar system can still function in such layout. However, the received power is reduced due to the longer signal path and weaker reflections from wall. In this experiment, the reference antenna was placed to the WiFi AP with an angle of 45° . Here, we provide a Doppler spectrogram for walking as shown in Fig. 20. Due to the weaker reference channel, Doppler signature is weaker than that in Figs. 10(i) and 15, but it is still clear and distinguishable. This spectrogram shows that our passive WiFi radar can tolerate the imperfect reference channel and provide similar results.

VII. CONCLUSION

In this article, we have demonstrated a passive WiFi radar system which uses a standalone WiFi AP. This system does not require any specific modification to hardware nor firmware, and it can work with any commercial WiFi AP. Two modes are implemented to cope the sparse beacon frame during the WiFi idle status. The sparse mode uses a modified CAF to extract the beacon frame based on the power profile, while it only provides limited Doppler detection. The modified CAF shows an average of 8-dB improvement comparing to classical CAF below 100 frame rate. Enhanced mode takes advantage of external client simulator which increases the throughput of WiFi signal. Enhanced mode can deliver similar performance as compared to the case with full transmission status. We have demonstrated the potential of the proposed system in

real-world deployment including the activity recognition (see Section VI-A), TTW breathing detection (see Section VI-B), and people counting (see Section VI-C). It is envisioned that a standalone WiFi sensing system can surpass current WiFi system which requires either high frame rate or specific system layout.

Future works include the implementation of WiFi decoder to replace the energy curve for a better synchronization. Also, a comparison between our passive radar system and CSI system would be very helpful to further explore the potential of WiFi sensing.

REFERENCES

- [1] C. J. Caspersen, K. E. Powell, and G. M. Christenson, "Physical activity, exercise, and physical fitness: Definitions and distinctions for health-related research," *Health Rep.*, vol. 100, no. 2, p. 126, 1985.
- [2] M. Amjadi, K.-U. Kyung, I. Park, and M. Sitti, "Stretchable, skin-mountable, and wearable strain sensors and their potential applications: A review," *Adv. Funct. Mater.*, vol. 26, no. 11, pp. 1678–1698, Mar. 2016.
- [3] S.-R. Ke, H. Thuc, Y.-J. Lee, J.-N. Hwang, J.-H. Yoo, and K.-H. Choi, "A review on video-based human activity recognition," *Computers*, vol. 2, no. 2, pp. 88–131, Jun. 2013.
- [4] A. Sciarrone, C. Fiandrino, I. Bisio, F. Lavagetto, D. Kliazovich, and P. Bouvry, "Smart probabilistic fingerprinting for indoor localization over fog computing platforms," in *Proc. 5th IEEE Int. Conf. Cloud Netw. (Cloudnet)*, Oct. 2016, pp. 39–44.
- [5] H. Abdelnasser, K. Harras, and M. Youssef, "Wigest: A ubiquitous WiFi-based gesture recognition system," in *Proc. Qatar Found. Annu. Res. Conf. Process.*, 2014, pp. 1472–1480.
- [6] Y. Wang, J. Liu, Y. Chen, M. Gruteser, J. Yang, and H. Liu, "E-eyes: Device-free location-oriented activity identification using fine-grained WiFi signatures," in *Proc. 20th Annu. Int. Conf. Mobile Comput. Netw.*, 2014, pp. 617–628.
- [7] W. Wang, A. X. Liu, M. Shahzad, K. Ling, and S. Lu, "Device-free human activity recognition using commercial WiFi devices," *IEEE J. Sel. Areas Commun.*, vol. 35, no. 5, pp. 1118–1131, May 2017.
- [8] W. Wang, A. X. Liu, and M. Shahzad, "Gait recognition using WiFi signals," in *Proc. ACM Int. Joint Conf. Pervas. Ubiquitous Comput.*, Sep. 2016, pp. 363–373.
- [9] H. Wang *et al.*, "Human respiration detection with commodity WiFi devices: Do user location and body orientation matter?" in *Proc. ACM Int. Joint Conf. Pervas. Ubiquitous Comput.*, Sep. 2016, pp. 25–36.
- [10] F. Colone, P. Falcone, C. Bongianni, and P. Lombardo, "WiFi-based passive bistatic radar: Data processing schemes and experimental results," *IEEE Trans. Aerosp. Electron. Syst.*, vol. 48, no. 2, pp. 1061–1079, Dec. 2012.
- [11] F. Colone, D. Pastina, P. Falcone, and P. Lombardo, "WiFi-based passive ISAR for high-resolution cross-range profiling of moving targets," *IEEE Trans. Geosci. Remote Sens.*, vol. 52, no. 6, pp. 3486–3501, Jun. 2014.
- [12] I. Milani, F. Colone, C. Bongianni, and P. Lombardo, "Impact of beacon interval on the performance of WiFi-based passive radar against human targets," in *Proc. 22nd Int. Microw. Radar Conf. (MIKON)*, May 2018, pp. 190–193.
- [13] Q. Chen, B. Tan, K. Chetty, and K. Woodbridge, "Activity recognition based on micro-Doppler signature with in-home Wi-Fi," in *Proc. IEEE 18th Int. Conf. e-Health Netw., Appl. Services (Healthcom)*, Sep. 2016, pp. 1–6.
- [14] W. Li, B. Tan, R. J. Piechocki, and I. Craddock, "Opportunistic physical activity monitoring via passive WiFi radar," in *Proc. IEEE 18th Int. Conf. e-Health Netw., Appl. Services (Healthcom)*, Sep. 2016, pp. 1–6.
- [15] W. Li, B. Tan, and R. J. Piechocki, "Non-contact breathing detection using passive radar," in *Proc. IEEE Int. Conf. Commun. (ICC)*, May 2016, pp. 1–6.
- [16] W. Li, B. Tan, Y. Xu, and R. J. Piechocki, "Log-likelihood clustering-enabled passive RF sensing for residential activity recognition," *IEEE Sensors J.*, vol. 18, no. 13, pp. 5413–5421, Jul. 2018.
- [17] K. Chetty, G. E. Smith, and K. Woodbridge, "Through-the-wall sensing of personnel using passive bistatic WiFi radar at standoff distances," *IEEE Trans. Geosci. Remote Sens.*, vol. 50, no. 4, pp. 1218–1226, Apr. 2012.

- [18] H. Wang, D. Zhang, Y. Wang, J. Ma, Y. Wang, and S. Li, "RT-fall: A real-time and contactless fall detection system with commodity WiFi devices," *IEEE Trans. Mobile Comput.*, vol. 16, no. 2, pp. 511–526, Feb. 2017.
- [19] S. Tan and J. Yang, "WiFinger: Leveraging commodity WiFi for fine-grained finger gesture recognition," in *Proc. 17th ACM Int. Symp. Mobile Ad Hoc Netw. Comput.*, 2016, pp. 201–210.
- [20] B. Tan, K. Woodbridge, and K. Chetty, "A real-time high resolution passive WiFi Doppler-radar and its applications," in *Proc. Int. Radar Conf.*, Oct. 2014, pp. 1–6.
- [21] W. Li, B. Tan, and R. Piechocki, "Passive radar for opportunistic monitoring in e-health applications," *IEEE J. Transl. Eng. Health Med.*, vol. 6, 2018, Art. no. 2800210.
- [22] R. V. Nee and R. Prasad, *OFDM For wireless Multimedia Communication*. Norwood, MA, USA: Artech House, 2000.
- [23] S. Markalous, S. Tenbohlen, and K. Feser, "Detection and location of partial discharges in power transformers using acoustic and electromagnetic signals," *IEEE Trans. Dielectrics Electr. Insul.*, vol. 15, no. 6, pp. 1576–1583, Dec. 2008.
- [24] *Ni Usrp 2921*. Accessed: Jul. 6, 2020. [Online]. Available: <http://sine.ni.com/nips/cds/view/p/lang/en/nid/212995>
- [25] Y. Ma, G. Zhou, and S. Wang, "WiFi sensing with channel state information: A survey," *ACM Comput. Surv.*, vol. 52, no. 3, p. 46, Jul. 2019.
- [26] Y. S. Lee, P. N. Pathirana, C. L. Steinfort, and T. Caelli, "Monitoring and analysis of respiratory patterns using microwave Doppler radar," *IEEE J. Transl. Eng. Health Med.*, vol. 2, 2014, Art. no. 1800912.
- [27] W. Xi *et al.*, "Electronic frog eye: Counting crowd using WiFi," in *Proc. IEEE Conf. Comput. Commun.*, Oct. 2014, pp. 361–369.
- [28] Y. LeCun *et al.*, "LeNet-5, convolutional neural networks," *Lenet*, vol. 20, no. 5, p. 14, 2015.



Wenda Li (Member, IEEE) received the M.Eng. and Ph.D. degrees from the University of Bristol, Bristol, U.K., in 2013 and 2017, respectively.

He worked with the University of Birmingham, Birmingham, U.K., as a Research Fellow before joining University College London, London, U.K., where he is a Research Fellow with the Department of Security and Crime Science. His research interests include the signal processing for passive radar and high-speed digital system design for wireless sensing applications in healthcare, security, and positioning.

His research in passive WiFi radar has led to a number of IEEE conference and journal publications.

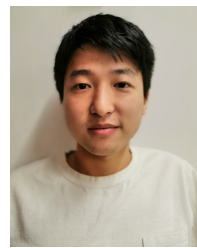


Robert J. Piechocki (Member, IEEE) is a Full Professor with the School of Computer Science, Electrical and Electronic Engineering and Engineering Maths, University of Bristol, Bristol, U.K. He is also a fellow with The Alan Turing Institute, London, U.K. His research interests include connected intelligent systems, wireless networks, information and communication theory, statistics, and machine learning. His domain expertise is connected and automated mobility (CAM) and wireless sensing for eHealth. In his research work, he strives to develop solutions for decision making and inference in networked systems which communicate over resource constrained and unreliable links. He has published over 200 papers in peer-reviewed international journals and conferences and holds 13 patents in these areas.



Karl Woodbridge (Senior Member, IEEE) is an Emeritus Professor of electronic and electrical engineering with University College London, London, U.K. His recent research interests include multistatic and software-defined radar systems, passive wireless surveillance, and Doppler classification using machine learning methods. His research interests include the development of passive wireless-based sensors for activity detection and classification with application to healthcare, Internet of Things, and security.

Dr. Woodbridge is a fellow of the Institution of Engineering and Technology (IET) and the U.K. Institute of Physics. He has served on technical and organizing committees for a wide range of international conferences and published or presented over 250 journal articles and conference papers in the areas of semiconductors, photonics, and RF sensor systems.



Chong Tang received the bachelor's degree in automation and electrical and electronic engineering from the University of Nottingham, Nottingham, U.K., in 2018, and the master's degree in robotics from University College London (UCL), London, U.K., in 2019. He is pursuing the Ph.D. degree with the Department of Security and Crime Science (SCS), UCL.

He is investigating the UCL Department of SCS to apply passive WiFi radar (PWR) system for occupancy detection and reconstruct human-skeletal model from Doppler-spectrogram-only data.



Kevin Chetty (Member, IEEE) is an Associate Professor with the Department of Security and Crime Science, University College London, London, U.K. His research interests include radio frequency (RF) sensing and radar signal processing using machine learning. His major achievements in RF sensing include demonstrating the first detections of personnel targets using passive WiFi radar and proving the ability of these systems to perform through-the-wall sensing at standoff distances. In the signal processing domain, his work has focused on classifying

people's actions based on their radar micro-Doppler signatures for applications in both security and e-healthcare. His work in this area also covers indoor mapping, target tracking, and high-throughput data processing. He is the author to over 50 peer-reviewed publications and has been an investigator on grants in passive wireless sensing and frequency-modulated continuous-wave (FMCW) radar for micro-Doppler target classification funded by EPSRC, EU Joint Research Centre, Ispra, Italy, U.K., Ministry of Defence/Defence Science and Technology Laboratory (Dstl), and the U.K. Maritime and Coastguard Agency, U.K.

Dr. Chetty is a member of Institution of Engineering and Technology (IET). He has served on the Technical and Organizing Committees for the IEEE Radar Conference and International Security and Crime Science Conference. He is also a reviewer for a number of high-esteem journals, including *IET Radar, Sonar and Navigation*, the *IEEE GEOSCIENCE AND REMOTE SENSING*, the *IEEE Communications Magazine*, and the *ACM Transactions on the Internet of Things (IoT)*.